

3 Conformal mapping

3.1 Wedges and channels

3.1.1 The basic idea

Suppose we wish to find the flow due to some given singularities (sources, vortices, *etc.*) in a region $R \subset \mathbb{C}$ with impermeable boundary ∂R . The idea is to perform a *conformal mapping* $\zeta = g(z)$ so that the region R in the z -plane is mapped to a much simpler region \hat{R} in the ζ -plane (for example a half-space). As shown schematically in Figure 3.1, any sources, vortices, *etc.* present in R will be mapped to corresponding singularities in \hat{R} . Now we can hopefully solve the transformed problem, for example using the method of images, to get the complex potential $W(\zeta)$. Then we just have to invert the conformal mapping to recover the complex potential in the original z -plane, namely

$$w(z) = W(g(z)). \quad (3.1)$$

We begin by illustrating the general approach using a simple example.

Example 3.1 *Source in a wedge*

Suppose fluid occupies the wedge-shaped region $0 < \theta < \alpha$, where θ is the usual polar angle, with impermeable walls on $\theta = 0$ and $\theta = \alpha$. We wish to find the flow due to a source of strength Q placed at a point $z = c$ inside the fluid (with $0 < \arg z < \alpha$ and $|c| > 0$).

We recall that the transformation

$$\zeta = g(z) = z^{\pi/\alpha} \quad (3.2)$$

maps the given wedge $0 < \arg z < \alpha$ onto the half-space $\text{Im } \zeta > 0$, and is conformal everywhere inside the wedge except at the origin. The source is mapped to the point $\zeta = c^{\pi/\alpha}$ which must lie somewhere in the half-space $\text{Im } \zeta > 0$.

The transformed problem of a source in a half-space is easily solved by the method of images, and the solution is found to be

$$W(\zeta) = \frac{Q}{2\pi} \log(\zeta - c^{\pi/\alpha}) + \frac{Q}{2\pi} \log(\zeta - \overline{c^{\pi/\alpha}}). \quad (3.3)$$

Now reversing the transformation, we find the complex potential

$$w(z) = W(z^{\pi/\alpha}) = \frac{Q}{2\pi} \log(z^{\pi/\alpha} - c^{\pi/\alpha}) + \frac{Q}{2\pi} \log(z^{\pi/\alpha} - \overline{c^{\pi/\alpha}}). \quad (3.4)$$

In particular, if we set $\alpha = \pi/2$, then (3.4) becomes

$$w(z) = \frac{Q}{2\pi} \log(z^2 - c^2) + \frac{Q}{2\pi} \log(z^2 - \bar{c}^2). \quad (3.5)$$

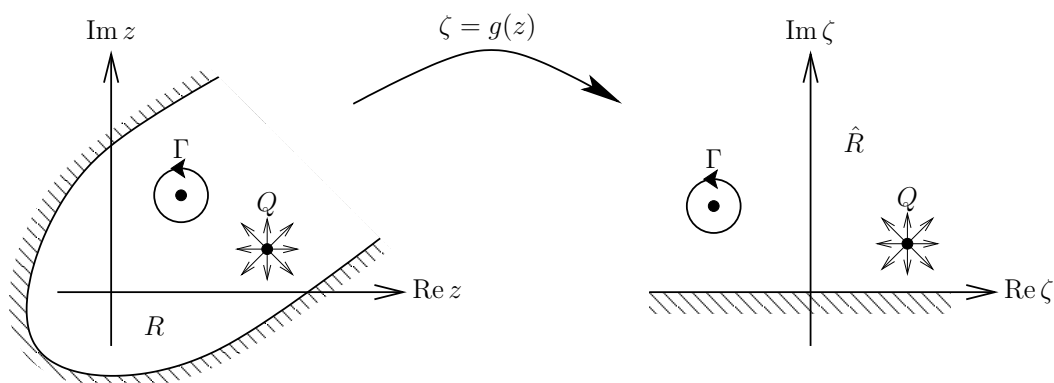


Figure 3.1: Schematic of a conformal mapping $\zeta = g(z)$ mapping a region R in the z -plane to the upper half-plane $\hat{R} = \{\zeta : \text{Im } \zeta > 0\}$ in the ζ -plane.

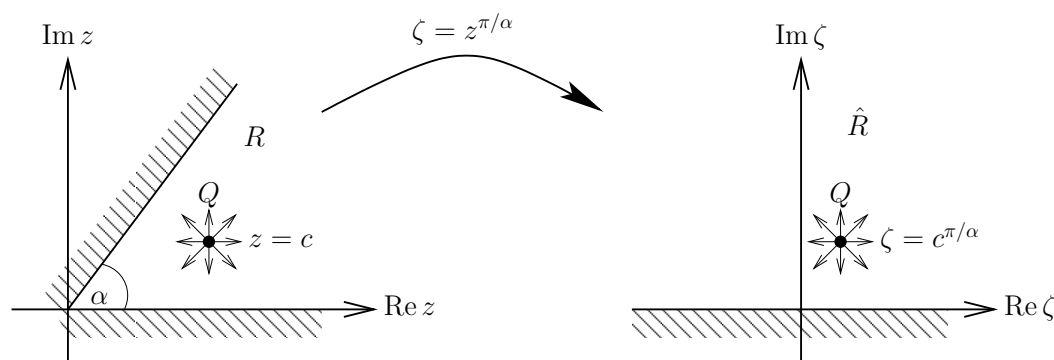


Figure 3.2: Schematic of the conformal mapping $\zeta = z^{\pi/\alpha}$ mapping the wedge $R = \{z : 0 < \arg z < \alpha\}$ in the z -plane to the upper half-plane $\hat{R} = \{\zeta : \text{Im } \zeta > 0\}$ in the ζ -plane.

The arguments of the logs are easily factorised to give

$$w(z) = \frac{Q}{2\pi} \log(z - c) + \frac{Q}{2\pi} \log(z + c) + \frac{Q}{2\pi} \log(z - \bar{c}) + \frac{Q}{2\pi} \log(z + \bar{c}), \quad (3.6)$$

which reproduces the result obtained for a quadrant in Section 2 by generalising the method of images.

3.1.2 Background theory

The above example illustrates the following important points that underpin the method.

1. **Conformal maps** are defined to be functions $\zeta = g(z)$ where $g(z)$ is *holomorphic* in R and $dg/dz \neq 0$ in R . We will be concerned with pairs of domains R and \hat{R} for which the map g defines a bijection between R and \hat{R} . The two domains are then said to be *conformally equivalent*.

2. Conformal maps **preserve angles**. We therefore expect the mapping not to be conformal at isolated *corners* in the boundary of R , where the angle is altered by the transformation. In Example 3.1, the mapping $\zeta = g(z)$ is not conformal at $z = 0$, where the angle is transformed from α to π .
3. If the boundary $\partial\hat{R}$ is a streamline in the ζ -plane, then the corresponding boundary ∂R is a streamline in the z -plane (and *vice versa*).

Proof If $\partial\hat{R}$ is a streamline, then $\text{Im} W(\zeta) = C$ for all $\zeta \in \hat{R}$, for some constant C . Since $\partial\hat{R}$ is the image of ∂R under the conformal mapping g , we can write $\partial\hat{R} = g(\partial R) = \{g(z) : z \in \partial R\}$. It follows that $\text{Im} w(z) = \text{Im} W(g(z)) = C$ for all $z \in \partial R$, and hence that ∂R is a streamline.

The converse result also holds since g is a bijection, so we can use exactly the same argument with g^{-1} . ■

4. A source of strength Q at $\zeta = g(c) \in \hat{R}$ in the ζ -plane corresponds to a source of *the same strength* Q at $z = c \in R$ in the z -plane (and *vice versa*).

Proof Suppose there is a source of strength Q at $\zeta = g(c) \in \hat{R}$, so that the complex potential takes the form

$$W(\zeta) \sim \frac{Q}{2\pi} \log(\zeta - g(c)) + O(1) \quad \text{as } \zeta \rightarrow g(c). \quad (3.7)$$

Since $z \mapsto g(z)$ is a bijection from R to \hat{R} , $\zeta \rightarrow g(c)$ if and only if $z \rightarrow c$, and it follows that

$$w(z) = W(g(z)) \sim \frac{Q}{2\pi} \log(g(z) - g(c)) + O(1) \quad \text{as } z \rightarrow c. \quad (3.8)$$

Furthermore, Taylor's Theorem gives

$$g(z) - g(c) \sim g'(c)(z - c) + O((z - c)^2) \quad \text{as } z \rightarrow c, \quad (3.9)$$

and hence

$$w(z) \sim \frac{Q}{2\pi} \log\left(g'(c)(z - c) + O((z - c)^2)\right) + O(1) \quad \text{as } z \rightarrow c, \quad (3.10)$$

where $g'(c) \neq 0$ since the mapping is supposed to be conformal. Therefore we can expand out the log to obtain

$$w(z) \sim \frac{Q}{2\pi} \log(z - c) + O(1) \quad \text{as } z \rightarrow c, \quad (3.11)$$

which implies the presence of a source of strength Q at $z = c$.

Again, the same argument works in reverse using g^{-1} instead of g . ■

Obviously, the same conclusion holds for vortices. However, the argument fails if we put a source or a vortex at a point where the mapping is not conformal, for example at an isolated corner in the boundary. Such cases require special treatment and will be avoided in this course.

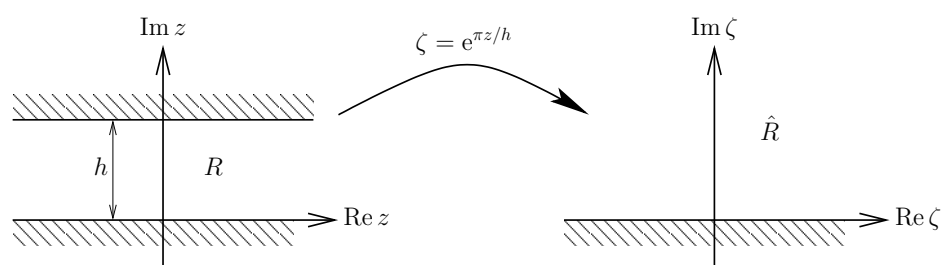


Figure 3.3: Schematic of the exponential conformal mapping $\zeta = e^{\pi z/h}$ mapping the channel $R = \{z : 0 < \text{Im } z < h\}$ in the z -plane to the upper half-plane $\hat{R} = \{\zeta : \text{Im } \zeta > 0\}$ in the ζ -plane.

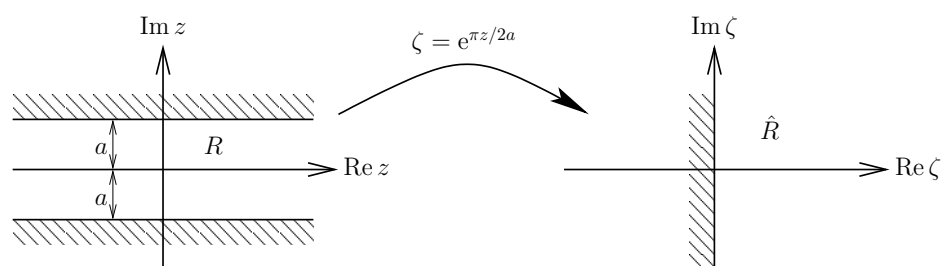


Figure 3.4: Schematic of the exponential conformal mapping $\zeta = e^{\pi z/2a}$ mapping the channel $R = \{z : -a < \text{Im } z < a\}$ in the z -plane to the right half-plane $\hat{R} = \{\zeta : \text{Re } \zeta > 0\}$ in the ζ -plane.

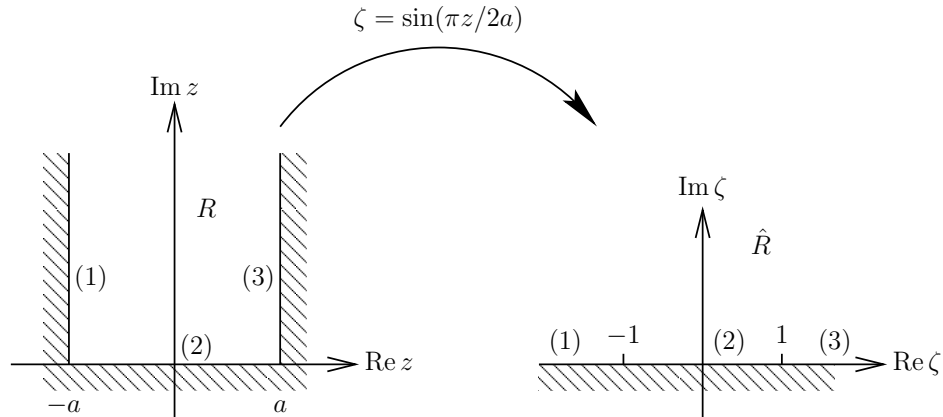


Figure 3.5: Schematic of the semi-infinite channel $R = \{z : \text{Im } z > 0, -a < \text{Re } z < a\}$ being transformed to the half-plane $\hat{R} = \{\zeta : \text{Im } \zeta > 0\}$ by the conformal mapping $\zeta = \sin(\pi z/2a)$.

3.1.3 Other examples of conformal maps

Exponential maps These are used to map a channel to a half-space. To start with, consider a channel of width h occupying the region $0 < \text{Im } z < h$ in the z -plane. The mapping

$$\zeta = g(z) = e^{\pi z/h} \quad (3.12)$$

maps this to the upper half-plane $\text{Im } \zeta > 0$, as shown schematically in Figure 3.3. We can easily see this by writing a typical point in R as $z = x + iy$, where $0 < y < h$. The corresponding point in \hat{R} is $\zeta = e^{\pi x/h} e^{i\pi y/h} = r e^{i\theta}$, where $r > 0$ and $0 < \theta < \pi$. Hence \hat{R} is the region $0 < \arg \zeta < \pi$, that is, the upper half-plane $\text{Im } \zeta > 0$.

The exponential mapping is easily generalised to deal with other channel-shaped regions. For example, the shifted channel $-a < \text{Im } z < a$ is transformed to the right half-plane $\text{Re } \zeta > 0$ by the mapping $\zeta = e^{\pi z/2a}$, as shown schematically in Figure 3.4.

Trigonometric maps These are used to map a semi-infinite channel onto a half-space. Consider for example the region R shown in Figure 3.5, where $\text{Im } z > 0$ and $-a < \text{Re } z < a$. The key observation is that, if we define

$$\zeta = g(z) = \sin\left(\frac{\pi z}{2a}\right), \quad (3.13)$$

then the mapping $z \mapsto g(z)$ is conformal everywhere in R and on ∂R , except at the corners $z = \pm a$, where dg/dz is zero. It is plausible, then, that this mapping may have the desired effect of “opening out” the angles of these corners and thus transforming ∂R into a straight line.¹ We can confirm that this is the case by considering the fates of the

¹The transformation (3.13) is an example of a so-called *Schwarz-Christoffel* mapping, a family of maps that can be used to map *any* simply-connected region of \mathbb{C} with a polygonal boundary to a half-plane.

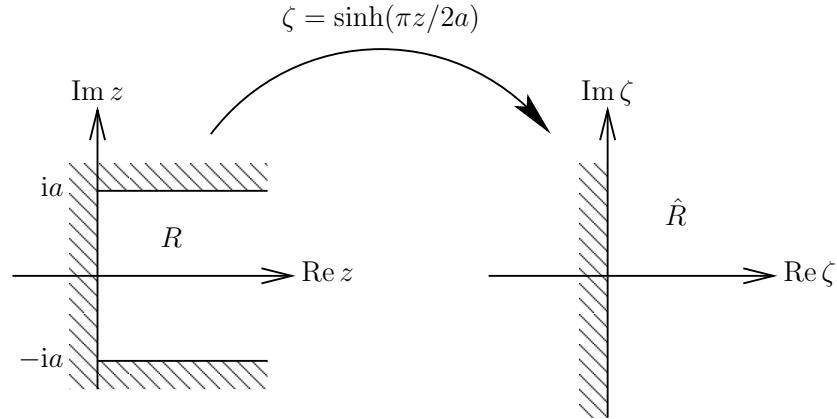


Figure 3.6: Schematic of the semi-infinite channel $R = \{z : \operatorname{Re} z > 0, -a < \operatorname{Im} z < a\}$ being transformed to the half-plane $\hat{R} = \{\zeta : \operatorname{Re} \zeta > 0\}$ by the conformal mapping $\zeta = \sinh(\pi z/2a)$.

three line segments marked (1), (2) and (3) in Figure 3.5.

We can parametrise line (1) by writing $z = -a + iy$, where $y > 0$. Its image is therefore parametrised by

$$\zeta = \sin\left(-\frac{\pi}{2} + i\frac{\pi y}{2a}\right) = -\cosh\left(\frac{\pi y}{2a}\right), \quad (3.14)$$

which traces out the segment of the real- ζ -axis from $-\infty$ to -1 , as indicated in Figure 3.5. On line (2), we have $z = x \in (-a, a)$ and hence

$$\zeta = \sin\left(\frac{\pi x}{2a}\right), \quad (3.15)$$

which parametrises in the interval $(-1, 1)$ on the real- ζ -axis. Finally, the image of line (3) is given by

$$\zeta = \sin\left(\frac{\pi}{2} + i\frac{\pi y}{2a}\right) = \cosh\left(\frac{\pi y}{2a}\right), \quad (3.16)$$

where $y > 0$, and this describes the segment $(1, \infty)$ on the real- ζ -axis.

These calculations establish that the boundary ∂R gets mapped to the real axis in the ζ -plane. It only remains to decide whether R is mapped to the upper or the lower half-plane, and this can be determined by considering just one point. For example, the point $z = i \in R$ is mapped to $\zeta = i \sinh(\pi/2)$, which has positive imaginary part, and it follows that the image of R is the upper half-plane $\operatorname{Im} \zeta > 0$, as indicated in Figure 3.5.

Other semi-infinite channel geometries can be handled using generalisations of (3.13). For example, the channel $\{z : \operatorname{Re} z > 0, -a < \operatorname{Im} z < a\}$ is transformed to the right half-plane by the mapping

$$\zeta = g(z) = \sinh(\pi z/2a), \quad (3.17)$$

as shown schematically in Figure 3.6. Again, the key to choosing the right map is to identify the corners where dg/dz should be zero.

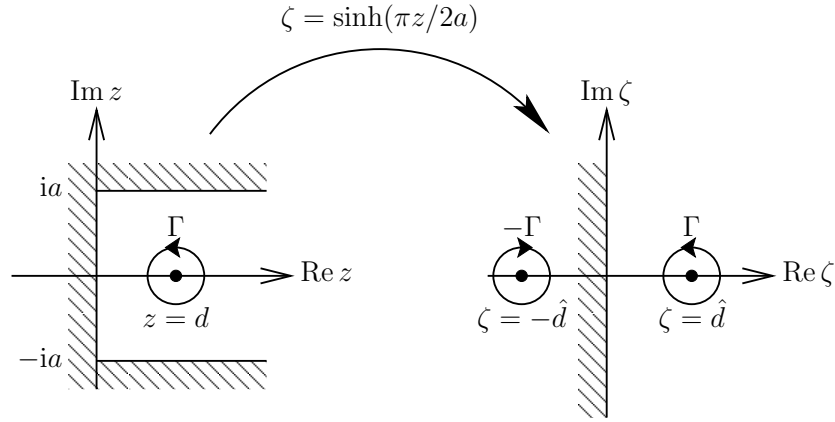


Figure 3.7: Schematic of a vortex at $z = d \in \mathbb{R}^+$ in the semi-infinite channel $R = \{z : \operatorname{Re} z > 0, -a < \operatorname{Im} z < a\}$ being transformed by the conformal mapping $\zeta = \sinh(\pi z/2a)$.

Example 3.2 A vortex in a semi-infinite channel

Consider the channel depicted in the left-hand z -plane in Figure 3.6. Now we wish to find the flow caused by the insertion of a vortex of strength Γ at the point $z = d \in \mathbb{R}^+$, as shown in Figure 3.7.

We use the mapping (3.17) to transform the channel on the right half-plane $\operatorname{Re} \zeta > 0$. The vortex at $z = d$ is mapped to $\zeta = \hat{d} = \sinh(\pi d/2a)$. We can then satisfy the boundary condition on the imaginary ζ -axis by inserting an equal and opposite vortex at the image point $\zeta = -\hat{d}$, as shown in Figure 3.7. The complex potential is thus given by

$$W(\zeta) = -\frac{i\Gamma}{2\pi} \log(\zeta - \hat{d}) + \frac{i\Gamma}{2\pi} \log(\zeta + \hat{d}), \quad (3.18)$$

or, in terms of the original complex variable z ,

$$w(z) = W(g(z)) = \frac{i\Gamma}{2\pi} \left\{ -\log\left(\sinh\left(\frac{\pi z}{2a}\right) - \hat{d}\right) + \log\left(\sinh\left(\frac{\pi z}{2a}\right) + \hat{d}\right) \right\}. \quad (3.19)$$

The velocity components are thus given by

$$u - iv = \frac{dw}{dz} = -\left(\frac{i\Gamma}{2a}\right) \left(\frac{\cosh(\pi z/2a) \sinh(\pi z/2a)}{\sinh^2(\pi z/2a) - \sinh^2(\pi d/2a)} \right), \quad (3.20)$$

and a little simplification leads to

$$u - iv = \frac{i\Gamma}{4a} \left\{ \operatorname{cosech}\left(\frac{\pi(z+d)}{2a}\right) - \operatorname{cosech}\left(\frac{\pi(z-d)}{2a}\right) \right\}. \quad (3.21)$$

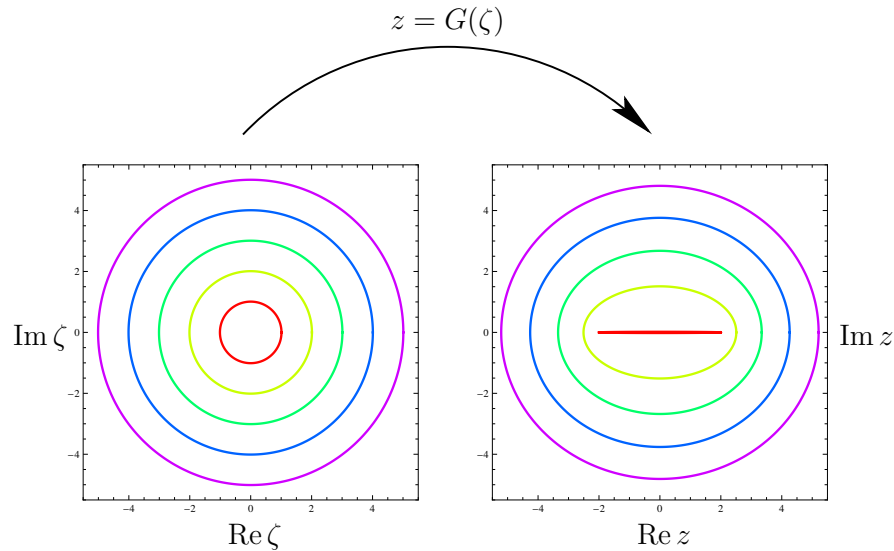


Figure 3.8: The images of circles $|\zeta| = r$ with $r \geq a$ under the Joukowski transformation $z = G(\zeta)$ given by (3.22). (Here $a = 1$.)

3.2 Aerofoil theory

3.2.1 The Joukowski Transformation

The *Joukowski transformation* is the map

$$z = G(\zeta) = \zeta + \frac{a^2}{\zeta} \quad (3.22)$$

from the complex ζ -plane to the z -plane, where a is a real parameter, which may be taken positive without loss of generality. The mapping $\zeta \mapsto G(\zeta)$ is conformal except at $\zeta = 0$ (where it has a pole) and at the points $\zeta = \pm a$ where $dG/d\zeta = 0$.

We can understand the general behaviour of the Joukowski transformation by considering its effect on the circle $|\zeta| = r$ in the ζ -plane. We can parametrise this circle by writing $\zeta = re^{i\theta}$, so that (3.22) becomes

$$z = re^{i\theta} + \frac{a^2}{r}e^{-i\theta} = \left(r + \frac{a^2}{r}\right) \cos \theta + i \left(r - \frac{a^2}{r}\right) \sin \theta. \quad (3.23)$$

Provided $r > a$, this describes an *ellipse* in the z -plane, with principle radii $r + a^2/r$ and $r - a^2/r$. In the limiting case $r \rightarrow a$, the ellipse degenerates to a line segment along the real z -axis, namely

$$S = \{z : \text{Im } z = 0, -2a \leq \text{Re } z \leq 2a\}. \quad (3.24)$$

As r varies between a and ∞ , these ellipses sweep out the entire complex z -plane, as shown in Figure 3.8. Hence the exterior of the circle $|\zeta| = a$ in the ζ -plane is mapped by the Joukowski transformation to the exterior of the line segment S .

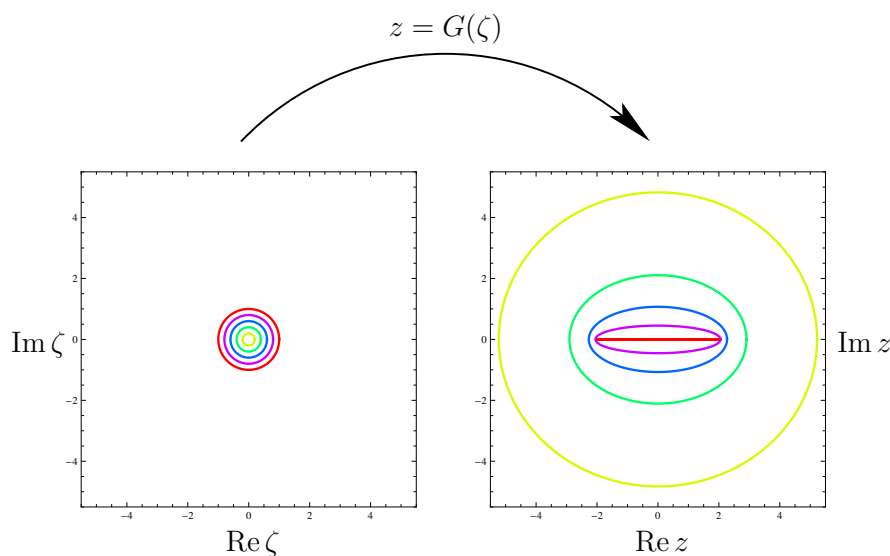


Figure 3.9: The images of circles $|\zeta| = r$ with $r \leq a$ under the Joukowski transformation $z = G(\zeta)$ given by (3.22). (Here $a = 1$.)

On the other hand, if $r < a$, (3.23) still parametrises an ellipse in the z -plane, now with principal radii $r + a^2/r$ and $a^2/r - r$ and now described in the clockwise rather than anticlockwise sense. As r varies between 0 and a , these ellipses again fill the entire complex z -plane, as shown in Figure 3.9, so the *interior* of the circle $|\zeta| = a$ also gets mapped to the exterior of the line segment S .

We can invert the Joukowski transformation (3.22) to obtain ζ as a function of z , namely

$$\zeta = \frac{1}{2} \left(z \pm \sqrt{z^2 - 4a^2} \right). \quad (3.25)$$

The square root term in (3.25) may be defined as

$$\sqrt{z^2 - 4a^2} = \sqrt{r_1 r_2} e^{i(\theta_1 + \theta_2)/2}, \quad (3.26)$$

where

$$r_1 = |z - 2a|, \quad r_2 = |z + 2a|, \quad \theta_1 = \arg(z - 2a), \quad \theta_2 = \arg(z + 2a) \quad (3.27)$$

are all shown schematically in Figure 3.10. The ranges for the angles are taken to be $-\pi < \theta_1, \theta_2 \leq \pi$, so the multifunction (3.26) is discontinuous across a branch cut along the line segment S on the real- z -axis.

By taking the + or the - in (3.25), we obtain two possible inverses for the mapping $\zeta \mapsto G(\zeta)$, namely

$$\zeta = g_+(z) = \frac{1}{2} \left(z + \sqrt{z^2 - 4a^2} \right), \quad \zeta = g_-(z) = \frac{1}{2} \left(z - \sqrt{z^2 - 4a^2} \right), \quad (3.28)$$

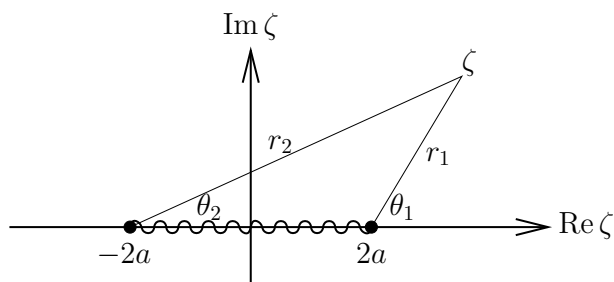


Figure 3.10: The lengths r_1 , r_2 and angles θ_1 , θ_2 used in the definition (3.26) of $\sqrt{z^2 - 4a^2}$.

both of which are conformal everywhere except on the line segment S . The function $g_+(z)$ maps the exterior of S to the exterior of the circle $|\zeta| = a$, while $g_-(z)$ maps the exterior of S to the interior of the circle $|\zeta| = a$, as indicated in Figure 3.11.

In Figure 3.12, we show the images in the z -plane of various circles in the ζ -plane. The first is the circle $|\zeta| = a$. This passes through the branch points $\zeta = \pm a$ (marked as red dots) where the Joukowski transformation is not conformal, and is mapped to the line segment S , as shown in diagram (i). The second circle, shown in diagram (ii), has a radius larger than a , and its image is thus an ellipse in the z -plane, as explained above. More interesting possibilities occur if we also shift the centre of the circle, as well as its radius. In diagram (iii), we illustrate the application of the Joukowski transformation to a circle whose centre has been slightly offset in the horizontal direction. We have chosen the radius such that the circle passes through one branch point $\zeta = a$, and this causes in a cusp at the corresponding point in the image. Finally, in diagram (iv) we show the result of shifting the circle both horizontally and vertically, while again choosing the radius so that it passes through $\zeta = a$. The resulting image has now lost both left-right and up-down symmetry, and still has a cusp at one end.

The shapes shown in the z -plane in diagrams (iii) and (iv) are examples of so-called *Joukowski aerofoils*. Shapes very similar to these are typically used as the cross-sections of aerofoils and other lifting bodies. They share the key features of a smooth *leading edge* and a sharp *trailing edge*.

The Joukowski transformation can be used to compute the complex potential for flow past any of the shapes shown in Figure 3.12. In this course, we will restrict our attention to case (i), which corresponds to a flat horizontal plate in the z -plane. The other cases are very similar in principle, but involve a few more tedious algebraic complications.

3.2.2 Uniform flow past a flat plate

Suppose fluid flows uniformly at speed U at angle of attack α past a flat plate of length $4a$ occupying the line segment $[-2a, 2a]$ along the real- z -axis. We can use the inverse Joukowski transformation $\zeta = g_+(z)$ to map the fluid onto the exterior of the circle $|\zeta| = a$, as shown schematically in Figure 3.13. The Circle Theorem allows us to calculate the complex potential in the ζ -plane, and the Joukowski transformation

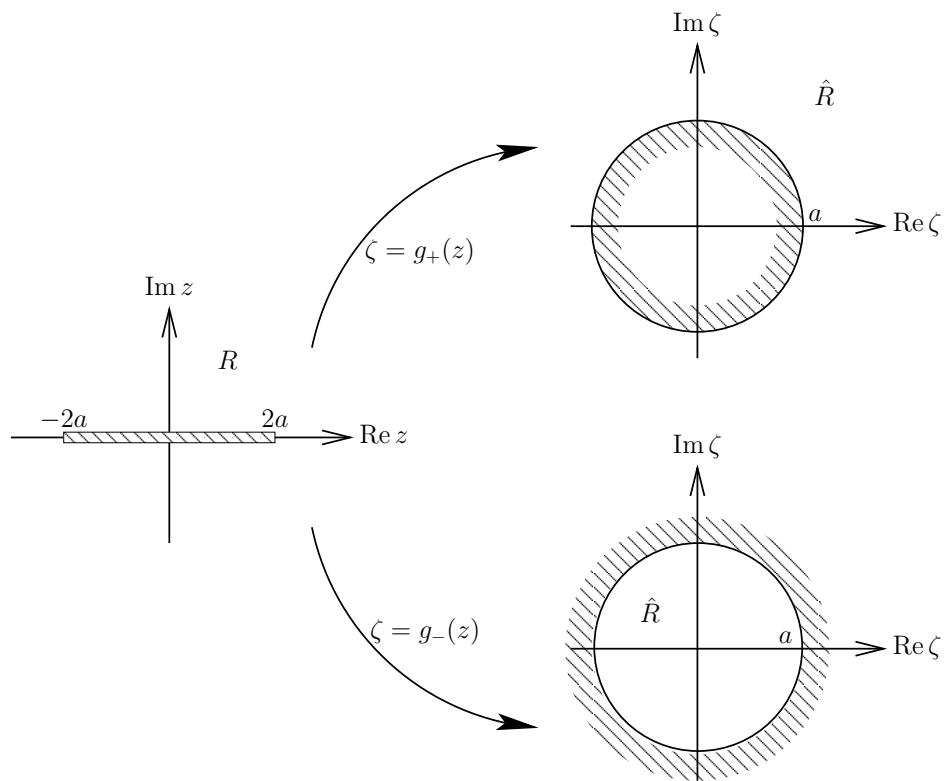


Figure 3.11: Schematic showing the exterior of the line segment $[-2a, 2a]$ along the real- z -axis being transformed by the conformal mappings $\zeta = g_+(z)$ and $\zeta = g_-(z)$ to the outside and inside respectively of the circle $|\zeta| = a$.

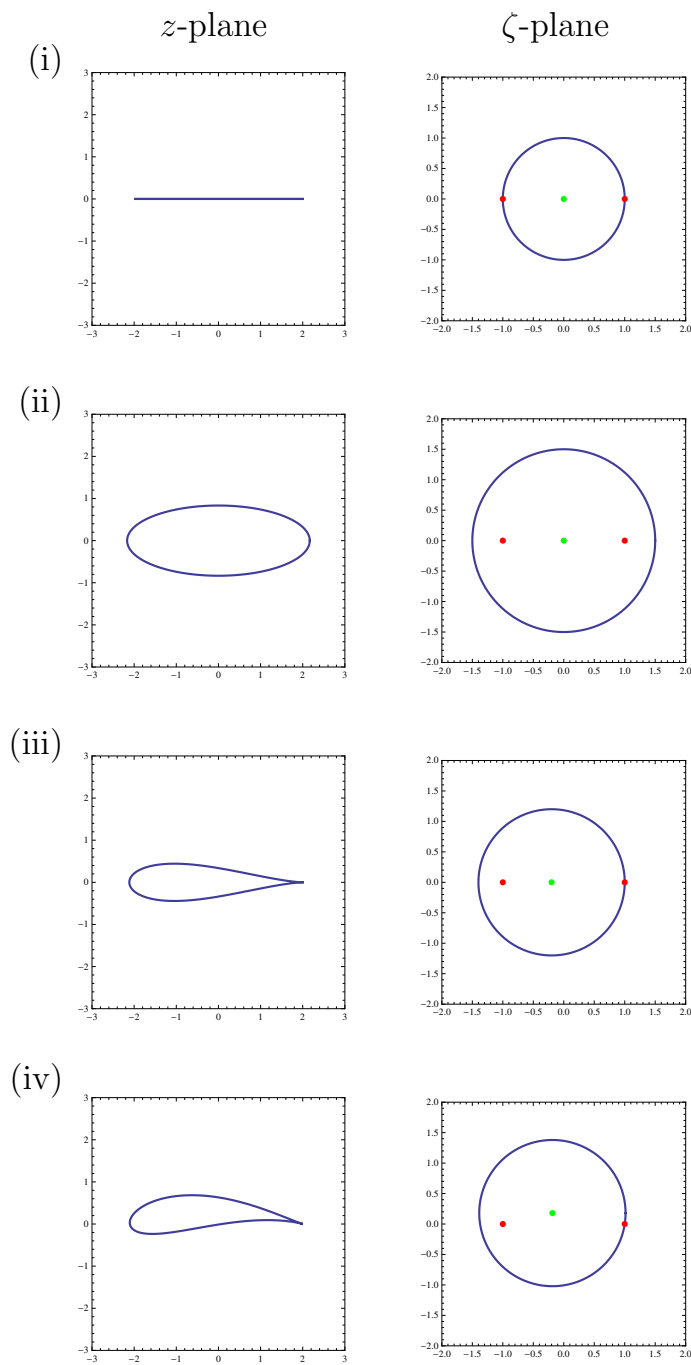


Figure 3.12: The images in the z -plane of four different circles in the ζ -plane under the Joukowski transformation. The centre of each circle is marked with a green dot. The red dots mark the points $\zeta = \pm a$ where the transformation is not conformal. (Here $a = 1$.)

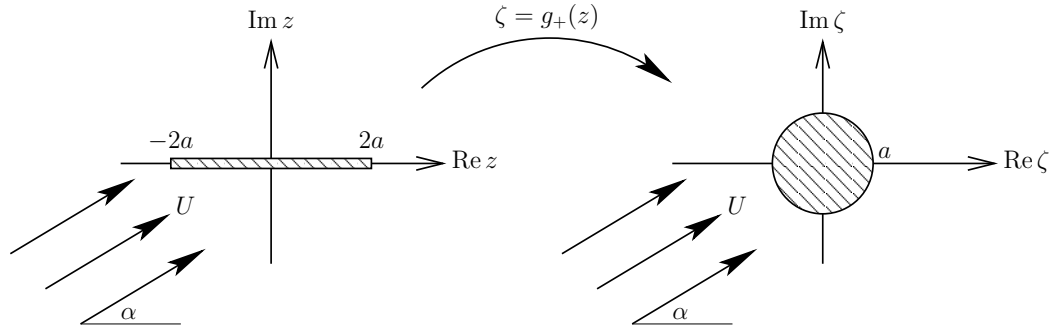


Figure 3.13: Schematic showing uniform flow past a flat plate in the z -plane being transformed to uniform flow past a circle in the ζ -plane by the conformal mapping $\zeta = g_+(z)$.

recovers the corresponding potential in the original z -plane.

Far from the plate, we require the flow to approach a uniform stream, and hence the complex potential should have the far-field behaviour

$$w(z) \sim Uze^{-i\alpha} \quad \text{as } z \rightarrow \infty. \quad (3.29)$$

We note from (3.22) and (3.25) that $\zeta \sim z$ as $z \rightarrow \infty$, and we therefore impose the corresponding behaviour

$$W(\zeta) \sim U\zeta e^{-i\alpha} \quad \text{as } \zeta \rightarrow \infty \quad (3.30)$$

on the complex potential in the ζ -plane.

Now the Circle Theorem, with background potential $f(\zeta) = U\zeta e^{-i\alpha}$, gives us the full complex potential in the ζ -plane, namely

$$W(\zeta) = U\zeta e^{-i\alpha} + \frac{Ua^2 e^{i\alpha}}{\zeta}. \quad (3.31)$$

The complex potential in the z -plane is given implicitly by (3.31) and the Joukowski mapping (3.22), and elimination of ζ leads to

$$\begin{aligned} w(z) &= \frac{Ue^{-i\alpha}}{2} \left(z + \sqrt{z^2 - 4a^2} \right) + \frac{Ue^{i\alpha}}{2} \left(z - \sqrt{z^2 - 4a^2} \right) \\ &= Uz \cos \alpha - iU \sqrt{z^2 - 4a^2} \sin \alpha. \end{aligned} \quad (3.32)$$

The velocity components are given by

$$u - iv = \frac{dw}{dz} = U \cos \alpha - \frac{iUz \sin \alpha}{\sqrt{z^2 - 4a^2}}. \quad (3.33)$$

The streamlines for the resulting flow are shown in Figure 3.14. We see that the flow is symmetric and the velocity is zero at two stagnation points $z = \pm 2a \cos \alpha$ on the plate.

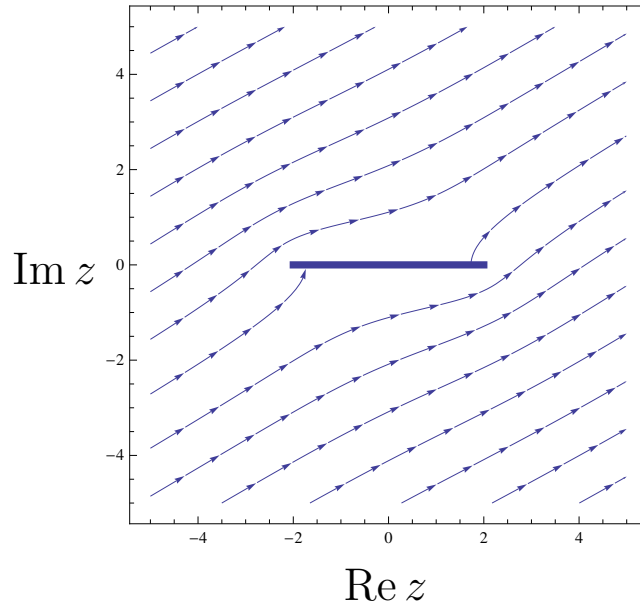


Figure 3.14: The streamlines for uniform flow with angle of attack α past a flat plate of length $4a$. (Here $\alpha = \pi/6$ and $a = 1$.)

We can incorporate a circulation Γ by inserting a vortex at the centre of the circle in the ζ -plane as usual, resulting in

$$W(\zeta) = U\zeta e^{-i\alpha} + \frac{Ua^2 e^{i\alpha}}{\zeta} - \frac{i\Gamma}{2\pi} \log \zeta. \quad (3.34)$$

Again we can eliminate ζ to obtain the complex potential $w(z)$ in the z -plane, although in practice this may not be worthwhile. We can instead calculate the velocity components by using the chain rule:

$$\begin{aligned} u - iv &= \frac{dw}{dz} = \frac{dW}{d\zeta} \bigg/ \frac{dz}{d\zeta} \\ &= \frac{Ue^{-i\alpha} - \frac{Ua^2 e^{i\alpha}}{\zeta^2} - \frac{i\Gamma}{2\pi\zeta}}{1 - \frac{a^2}{\zeta^2}} \\ &= \frac{Ue^{-i\alpha}\zeta^2 - i(\Gamma/2\pi)\zeta - Ua^2 e^{i\alpha}}{\zeta^2 - a^2}. \end{aligned} \quad (3.35)$$

Now the stagnation points in the ζ -plane are given by

$$\frac{\zeta}{a} = e^{i\alpha} \left(i\gamma \pm \sqrt{1 - \gamma^2} \right), \quad (3.36)$$

where we recall the shorthand $\gamma = \Gamma/4\pi Ua$. Provided $\gamma \in (-1, 1)$, there are two stagnation points, both lying on the circle $|\zeta| = a$. We use the Joukowski transformation (3.22) to map these back to two stagnation points on the plate in the z -plane given by

$$z = 2a \left(-\gamma \sin \alpha \pm \sqrt{1 - \gamma^2} \cos \alpha \right). \quad (3.37)$$

We see that these revert to their zero-circulation positions $z = \pm 2a \cos \alpha$ when $\gamma = 0$.

Alternatively, we can eliminate ζ to write the complex potential in the z -plane as

$$Uz \cos \alpha - iU \sqrt{z^2 - 4a^2} \sin \alpha - \frac{i\Gamma}{2\pi} \log \left(\frac{z + \sqrt{z^2 - 4a^2}}{2} \right). \quad (3.38)$$

Now differentiation with respect to z and simplification leads to

$$u - iv = \frac{dw}{dz} = U \cos \alpha - \frac{i}{\sqrt{z^2 - 4a^2}} \left(\frac{\Gamma}{2\pi} + Uz \sin \alpha \right). \quad (3.39)$$

3.2.3 The Kutta condition

We can see from equation (3.39) that the velocity is in general unbounded at the two edges of the plate $z = \pm 2a$. In practice, viscous effects will come into play in a neighbourhood of the edges of the plate to ensure that the velocity remains finite. With these effects included, it turns out to be impossible for the fluid to bend around the trailing edge of the plate, as indicated by Figure 3.14. Instead it must separate smoothly as shown in Figure 3.15, and this selects a particular value of the circulation Γ . The *Kutta condition* states that the circulation must be chosen such that *the velocity at the trailing edge is finite*.

Returning to equation (3.39), we see that the velocity at the trailing edge can be finite only if the final bracketed term tends to zero as $z \rightarrow 2a$, and this implies that the circulation must be given by

$$\Gamma = -4\pi Ua \sin \alpha. \quad (3.40)$$

Having made this choice, we can then evaluate the velocity at the trailing edge from (3.39), for example by using l'Hôpital's rule:

$$u - iv|_{z=2a} = \left. \frac{dw}{dz} \right|_{z=2a} = U \cos \alpha. \quad (3.41)$$

Hence we see that the fluid velocity is tangent to the plate at the trailing edge, as shown in Figure 3.15.

Of course, the velocity is still unbounded at the *leading* edge of the plate $z = -2a$. This is a problem with flow past a flat plate, and partly explains why flat plates do not make particularly good aerofoils. More realistic aerofoil shapes have a smooth leading edge and a sharp trailing edge, like those shown in Figure 3.12(iii) and (iv). For such shapes, the Kutta condition gives rise to a velocity field that is bounded everywhere.

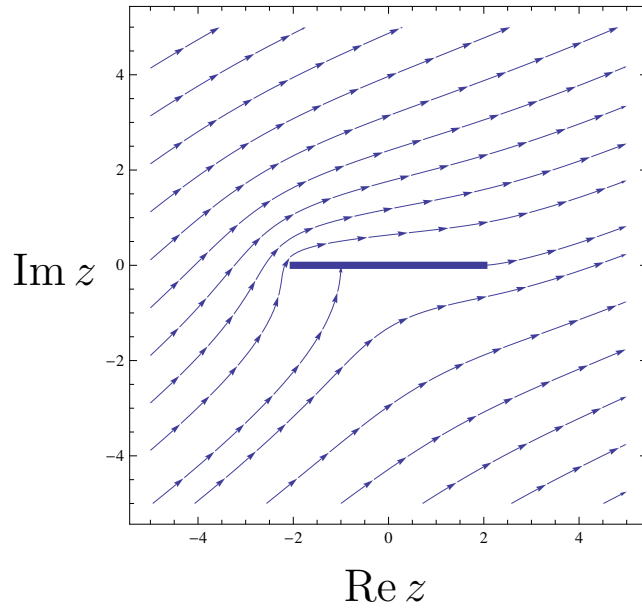


Figure 3.15: The streamlines for uniform flow with angle of attack α past a flat plate of length $4a$, with circulation given by (3.40) to satisfy the Kutta condition. (Here $\alpha = \pi/6$ and $a = 1$.)

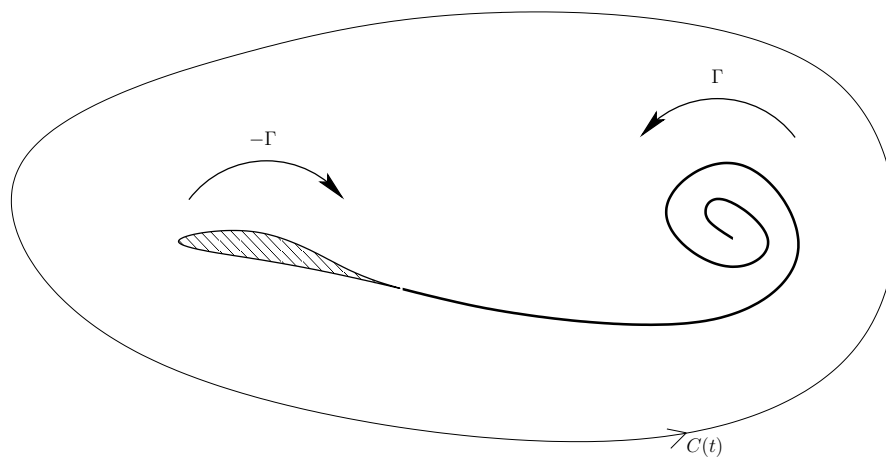


Figure 3.16: Schematic of a trailing vortex behind an aerofoil. The material curve $C(t)$ encloses both the vortex and the aerofoil.

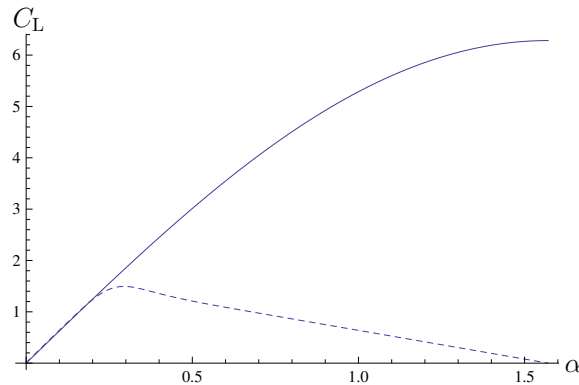


Figure 3.17: Lift coefficient C_L for a flat plate versus angle of attack α . The solid curve shows the theoretical prediction $C_L = 2\pi \sin \alpha$ implied by (3.42); the dashed curve shows schematically typical experimental results.

We recall from Kelvin’s Circulation Theorem that the circulation around a closed material curve $C(t)$ is constant in time. This raises the question: how did the circulation (3.40) around the plate arise in the first place? The answer is that, as an aerofoil accelerates from rest, the Kutta condition forces it to shed a *starting vortex*, as shown schematically in Figure 3.16.² By applying Kelvin’s Theorem to a large contour $C(t)$ that encloses both the aerofoil and the starting vortex, we deduce that there must be a circulation around the aerofoil equal and opposite to that around the starting vortex.

Once we have used the Kutta condition to determine the circulation around an aerofoil, we can apply the Kutta–Joukowski Lift Theorem to calculate the lift and drag forces, namely $L = -\rho U \Gamma$, $D = 0$. For a flat plate, the circulation is given by equation (3.40), and the resulting lift force is therefore given by

$$L = 4\pi\rho U^2 a \sin \alpha. \quad (3.42)$$

Wind-tunnel experiments show that this formula works very well provided the angle of attack α is smaller than about $\pi/12$. If α is increased any further, the lift rapidly decreases to virtually zero, and the aerofoil *stalls*. This is caused by the formation of a turbulent wake downstream of the aerofoil.

We illustrate this behaviour in Figure 3.17. The lift on the plate is measured by the dimensionless *lift coefficient*

$$C_L = \frac{L}{2\rho U^2 a}, \quad (3.43)$$

where equation (3.42) implies that $C_L = 2\pi \sin \alpha$. As shown by the solid curve in Figure 3.17, the theoretically predicted lift increases with the angle of attack, attaining its maximum value as $\alpha \rightarrow \pi/2$. However, it is intuitively clear that the lift should be zero when the plate is aligned transverse to the flow. Typical experimental results are shown schematically by the dashed curve.

²These vortices dictate the time delay between aeroplanes taking off from a busy airport.

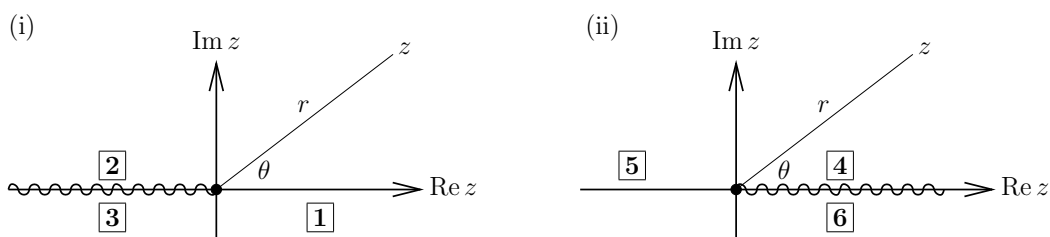


Figure 3.18: The cut complex plane for $\arg z = \theta$ when we choose (i) $\theta \in [-\pi, \pi]$; (ii) $\theta \in [0, 2\pi]$ The six regions $\boxed{1}$ – $\boxed{6}$ labelled along the real- z -axis are described in the text.

3.3 Background material: multifunctions

We can write any complex number z in terms of its modulus $r = |z|$ and argument $\theta = \arg z$ as

$$z = re^{i\theta}. \quad (3.44)$$

The argument θ is simply the polar angle of the point (x, y) in the Argand plane representing the complex number $z = x + iy$. As such, it is not uniquely defined. For example, the complex number -1 may be written in the form (3.44) with $r = 1$ and $\theta = (2n + 1)\pi$ for any integer n . Hence $\theta = \arg z$ is a *multifunction*, taking each value of z to multiple possible values of θ . To define $\arg z$ uniquely, we must pick an interval of length 2π in which it must lie. This process is known as *choosing a branch* for the multifunction $\arg z$.

For example, we might insist that θ lie in the interval $[-\pi, \pi]$. This would select a unique value of θ corresponding to each nonzero value of z , apart from the negative real axis, where θ could be π or $-\pi$. The line along which the value of $\arg z$ is ambiguous is called a *branch cut*, and is marked as a wiggly line in Figure 3.18(i).

Let us consider the values of $\arg z$ on the three regions along the real- z -axis marked $\boxed{1}$ – $\boxed{3}$ in Figure 3.18(i). On the positive real axis $\boxed{1}$, we simply have $\theta = 0$. However, on the negative real axis, the value of θ is π if we approach from above $\boxed{2}$ or $-\pi$ if we approach from below $\boxed{3}$. Hence, the price that we pay for uniqueness is that θ suffers a discontinuity across the branch cut.

Of course, this particular choice for the range of θ is far from unique; for example, we could instead have chosen $\theta \in [0, 2\pi]$. The branch cut would then be along the positive real axis, as shown in Figure 3.18(ii), and the value of $\arg z$ on the negative real axis $\boxed{5}$ would unambiguously be equal to π . Instead, we would now have a discontinuity in $\arg z$ across the positive real axis, from 0 when approached from above $\boxed{4}$ to 2π when approached from below $\boxed{6}$.

Next, consider the function \sqrt{z} , where $z \in \mathbb{C}$. By writing z in the polar form (3.44), we can define the square root as

$$\sqrt{z} = \sqrt{r} e^{i\theta/2}, \quad (3.45)$$

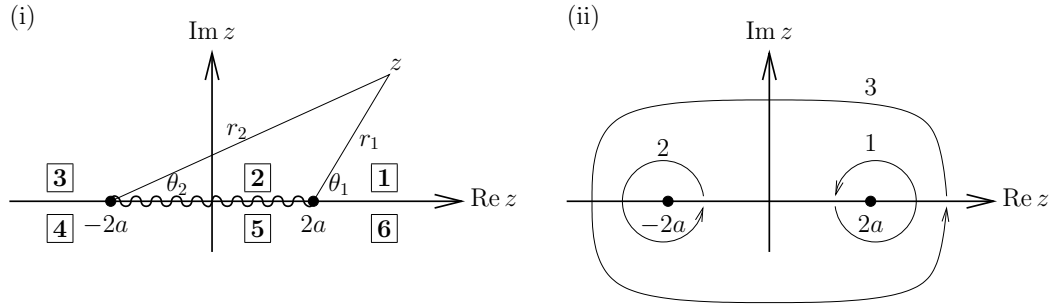


Figure 3.19: (i) Six regions $\boxed{1}$ – $\boxed{6}$ along the real- z -axis illustrating the branch cut in the function $\sqrt{z^2 - 4a^2}$. (ii) Three possible closed circuits in the z -plane: 1 enclosing $z = 2a$; 2 enclosing $z = -2a$; 3 enclosing both $z = 2a$ and $z = -2a$.

where \sqrt{r} is the usual real (positive) square root. Equation (3.45) allows us to define \sqrt{z} uniquely once $\arg z$ has been defined uniquely, and again we have to choose a branch.

Suppose, for example, we choose the branch with $\theta \in [-\pi, \pi]$, as shown in Figure 3.18(i). Along the positive real axis $\boxed{1}$ we have $z = x > 0$ and $\theta = 0$ so that $\sqrt{z} = \sqrt{x} > 0$. Approaching the negative real axis from above $\boxed{2}$, we have $z = x < 0$ and $\theta = \pi$, so that $\sqrt{z} = i\sqrt{-x}$. On the other hand, if we approach the negative real axis from below $\boxed{3}$, then $\theta = -\pi$ and therefore $\sqrt{z} = -i\sqrt{-x}$. Hence \sqrt{z} suffers a discontinuity of $2i\sqrt{|z|}$ as the branch cut is crossed.

Finally we consider the function $\sqrt{z^2 - 4a^2}$. By writing

$$z^2 - 4a^2 = (z - 2a)(z + 2a) = r_1 r_2 e^{i(\theta_1 + \theta_2)}, \quad (3.46)$$

where the lengths r_1, r_2 and angles θ_1, θ_2 are defined by

$$r_1 = |z - 2a|, \quad r_2 = |z + 2a|, \quad \theta_1 = \arg(z - 2a), \quad \theta_2 = \arg(z + 2a), \quad (3.47)$$

and shown schematically in Figure 3.19(i), we can define

$$\sqrt{z^2 - 4a^2} = \sqrt{r_1 r_2} e^{i(\theta_1 + \theta_2)/2}. \quad (3.48)$$

Now we must choose branches for θ_1 and θ_2 . Suppose we perform a small closed circuit around the point $z = 2a$ in the complex plane, for example the path marked 1 in Figure 3.19(ii). When the circuit is completed, θ_1 will have increased by a multiple of 2π , while θ_2 will be unchanged. We deduce from (3.46) that the sign of $\sqrt{z^2 - 4a^2}$ must switch between one end of the circuit and the other. Similarly, if we follow circuit 2, enclosing $z = -2a$, then θ_2 will increase by a factor of 2π while θ_1 is unchanged, and again there will therefore be a discontinuity in $\sqrt{z^2 - 4a^2}$.

However, if we perform a circuit of *both* $z = a$ and $z = -a$, as indicated by path 3, then both θ_1 and θ_2 increase by a factor of 2π , as therefore does $(\theta_1 + \theta_2)/2$. Such a circuit hence returns $\sqrt{z^2 - 4a^2}$ to its starting value. We deduce that $\sqrt{z^2 - 4a^2}$ must suffer a discontinuity if *either* $z = 2a$ or $z = -2a$ is encircled, but *not* if they both are.

We therefore only need to cut the complex plane along a line joining $z = -2a$ to $z = 2a$, as shown in Figure 3.19(i).

Suitable choices for the branches are $\theta_1, \theta_2 \in [-\pi, \pi]$. Let us then examine the values of $\sqrt{z^2 - 4a^2}$ in the six regions marked **1**–**6** along the real- z -axis in Figure 3.19(i).

- In region **1**, where $z = x > a$, we have $\theta_1 = \theta_2 = 0$ and hence

$$\sqrt{z^2 - 4a^2} = \sqrt{x - a}\sqrt{x + a}.$$

- In region **2**, where $z = x \in (-a, a)$, and we approach from above, we have $\theta_1 = \pi$, $\theta_2 = 0$ and hence

$$\sqrt{z^2 - 4a^2} = i\sqrt{a - x}\sqrt{x + a}.$$

- In region **3**, where $z = x < -a$, and we approach from above, we have $\theta_1 = \pi$, $\theta_2 = \pi$ and hence

$$\sqrt{z^2 - 4a^2} = -\sqrt{a - x}\sqrt{-a - x}.$$

- In region **4**, where $z = x < -a$, and we approach from below, we have $\theta_1 = -\pi$, $\theta_2 = -\pi$ and hence

$$\sqrt{z^2 - 4a^2} = -\sqrt{a - x}\sqrt{-a - x}.$$

Notice that there is no discontinuity between regions **3** and **4**.

- In region **5**, where $z = x \in (-a, a)$, and we approach from below, we have $\theta_1 = -\pi$, $\theta_2 = 0$ and hence

$$\sqrt{z^2 - 4a^2} = -i\sqrt{a - x}\sqrt{x + a}.$$

Notice that there *is* a discontinuity between regions **2** and **5**.

- In region **6**, we have $\theta_1 = \theta_2 = 0$ and hence

$$\sqrt{z^2 - 4a^2} = \sqrt{x - a}\sqrt{x + a},$$

exactly as in region 1.